Final States with One or Two Charged Particles and a Visible $\bar{K}^0$ from K^-d Interactions at 4.5 GeV/c*

D. D. Carmony, R. L. Eisner,†‡ A. C. Ammann, A. F. Garfinkel, L. J. Gutay, D. H. Miller, and L. K. Rangan

Physics Department, Purdue University, Lafayette, Indiana 47907

AND

W. L. Yen

Physics Department, Indiana University-Purdue University at Indianapolis, Indianapolis, Indiana 46205

(Received 16 February 1970)

We report on a study of the interactions of 4.48-GeV/c K^- mesons on deuterium. The 372 000-picture exposure was taken in the Argonne National Laboratory 30-in. deuterium-filled bubble chamber. The $\bar{K}^0$ final states from the one- and two-prong-plus-vee topologies are discussed. The final states investigated include (1) $\bar{K}^0\pi^-pn$, (2) $\bar{K}^0\pi^-d$, (3) $\bar{K}^0\pi^-\pi^0d$, (4) $\bar{K}^0\pi^-p$ (missing mass). Production of the $K^{*-}(890)$ resonance is analyzed from both K^--proton and K^--neutron interactions and is compared with absorption and Regge-pole models. The production of $\Delta^-(1236)$ in reaction (1) is compared with the predictions of Thews and with those of Maor and Krammer. Strong $K^{*-}(890)$ production occurs in reaction (2), and evidence for dominant-vector-meson exchange is given. The d^* enhancement is quite strong in (3), and K^*d^* production is discussed.

I. INTRODUCTION

IN recent years, a wide range of information about resonance production has come from the inelastic scattering of charged kaons on nucleons. The discovery of the vector[1] $K^*(890)$ and the tensor[2] $K^*(1400)$ mesons provided the impetus for the examination of their production and decay properties in other experiments. The purpose of the present experiment is to explore further the properties of resonance production in K^- nucleon reactions. The data for this analysis were obtained from a 372 000-picture exposure in the ANL 30-in. deuterium bubble chamber at an incident K^- momentum of 4.48 GeV/c. Except for a contamination of about 2% muons, the beam was essentially pure kaons.[3]

The film was scanned for events of the type one- or two-prongs-plus-vee. This paper is limited to those events in which the vee is a $\bar{K}^0$. The Λ final states are discussed in a previous article.[3] The reactions investigated include

$$K^-d \rightarrow \bar{K}^0\pi^-pn \tag{1}$$

$$\rightarrow \bar{K}^0\pi^-d \tag{2}$$

$$\rightarrow \bar{K}^0\pi^-\pi^0d \tag{3}$$

$$\rightarrow p\bar{K}^0\pi^-\text{MM}, \tag{4}$$

where MM denotes missing neutrals. Preliminary reports from this experiment have been presented earlier.[4,5]

II. EXPERIMENTAL DETAILS

The film was scanned twice for events of the type one- and two-prong-plus-vee. In the case of the two-prong events, we demanded that the positive particle have a range of less than 15 cm.
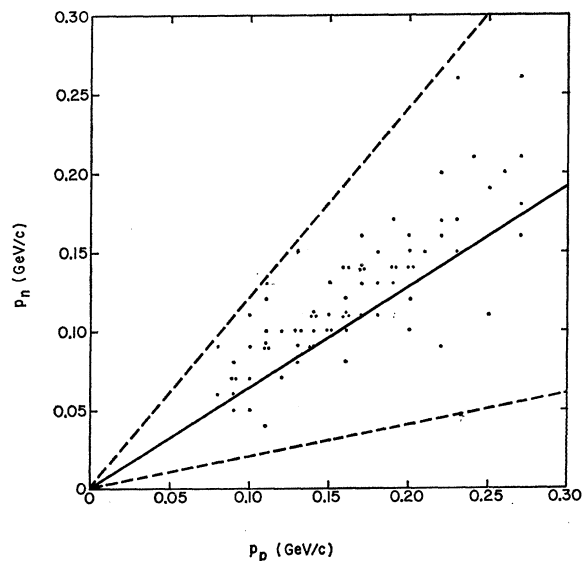

FIG. 1. Scatter plot of the neutron momentum versus the proton momentum for the events of reaction (2) when interpreted as reaction (1). The solid line is the predicted curve ($p_n/p_p = 0.64$). The dashed lines define the region $0.2 < p_n/p_p < 1.2$.

[1] M. Alston, L. Alvarez, P. Eberhard, M. L. Good, W. Graziano, H. K. Ticho, and S. G. Wojcicki, Phys. Rev. Letters 6, 300 (1961).

[2] Birmingham-Glasgow-London (I.C.)-Oxford-Rutherford Collaboration, Phys. Letters 14, 338 (1965).

[3] W. L. Yen, A. C. Ammann, D. D. Carmony, R. L. Eisner, A. F. Garfinkel, L. J. Gutay, S. L. Kramer, and D. H. Miller, Phys. Rev. 188, 2011 (1969).

[4] R. L. Eisner, A. C. Ammann, D. D. Carmony, A. F. Garfinkel, L. J. Gutay, R. V. Lakshmi, D. H. Miller, G. W. Tautfest, and W. L. Yen, Phys. Letters 28B, 356 (1968).

[5] D. D. Carmony, H. W. Clopp, A. F. Garfinkel, L. J. Gutay, D. H. Miller, and R. L. Eisner, Nucl. Phys. B12, 9 (1969).
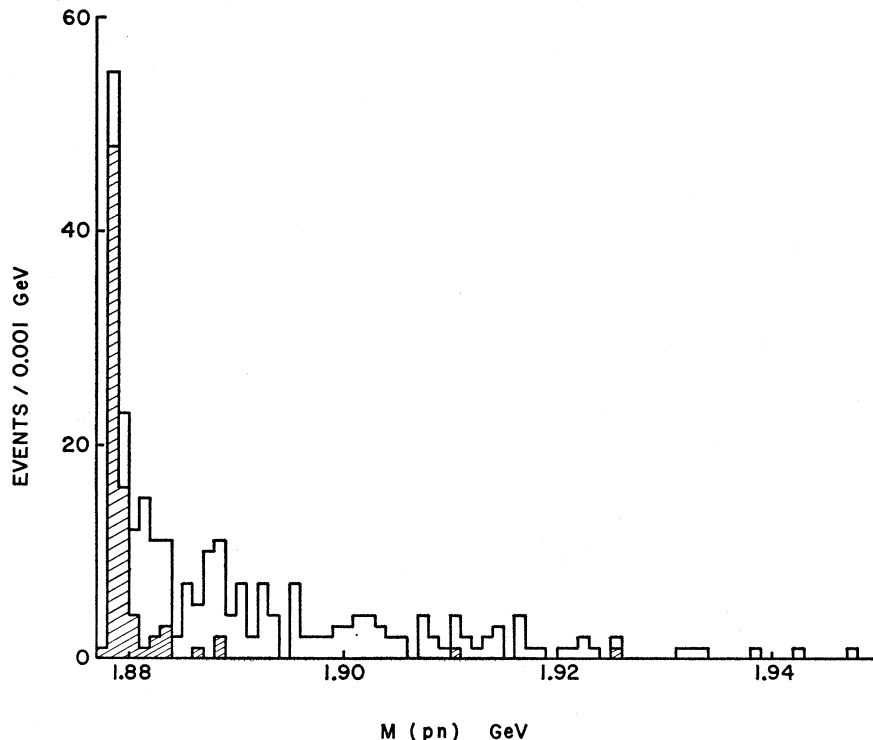
FIG. 2. Proton-neutron effective mass for events which fit reaction (1) with the ratio of the neutron momentum to the proton momentum in the range 0.2–1.2. The shaded events also fit reaction (2).

All events of these topologies were measured on three scanning and measuring projectors (SMP) on line to an IBM 360/40-44 system which provided geometric reconstruction (TVGP). The kinematic fitting was performed on the IBM 360/44 using the Berkeley program SQUAW.

The deuteron events were required to have a visible outgoing positive track, and thus the study of reactions (2) and (3) is limited to events where the deuteron has a laboratory momentum of at least 150 MeV/c.

Events with an acceptable fit to reaction (2) also fitted reaction (1) except for three events where the positive track was unambiguously identified as a deuteron. However, the following considerations can be used to identify the $\bar{K}^0\pi^-d$ final state:

(1) If the deuteron fit is to be faked by that of the proton-neutron hypothesis, in which the only momentum information comes from the range of the proton, the ratio of neutron to proton momentum (p_n/p_p) is kinematically constrained to be approximately 0.64.[6] In Fig. 1, we plot the neutron momentum against the proton momentum for events selected as deuteron fits. The solid line is $p_n/p_p=0.64$. The scattering of events about the line is consistent with our measurement error.

(2) Figure 2 gives the effective-mass distribution of the pn combination for all events that fit reaction (1) and for which p_n/p_p was between 0.2 and 1.2. The peak

between 1.878 and 1.880 GeV overwhelmingly comes from the events of reaction (2) which are shown shaded in Fig. 2.

(3) Since we have found that reactions (2) and (3) are dominated by $K^{*-}(890)$ production, we have generated Monte Carlo events[7] to find the number of events from the reaction

$$K^-d \rightarrow K^{*-}(890)np \qquad (5)$$

which could fake

$$K^-d \rightarrow K^{*-}(890)d. \qquad (6)$$

We found an expected contamination from reaction (5) to reaction (6) of less than one event.

Thus all 83 events that satisfied reaction (2) with a confidence level of more than 1% and had a visible positive prong were classified as deuteron events. The events that have an acceptable χ^2 for reaction (2) with an unseen deuteron have also been examined. Our analysis of these 90 events indicates a contamination of more than 50%, and hence these events have not been used in the subsequent analysis of reaction (2). They are included in the $\bar{K}^0\pi^-pn$ sample.

Figure 3 gives the missing-mass distribution from the reaction

$$K^-d \rightarrow \bar{K}^0\pi^-p\mathrm{MM}, \qquad (4)$$

[6] M. A. Abolins, Ph.D. thesis, University of California at San Diego, La Jolla, Calif., 1965 (unpublished).

[7] We used the Berkeley program FAKE: G. R. Lynch, UCRL Report No. UCRL-10335 (1962). A momentum-transfer cut between the incident K^- and the outgoing $K^{*-}(890)$ of the form e^{3t} was imposed.
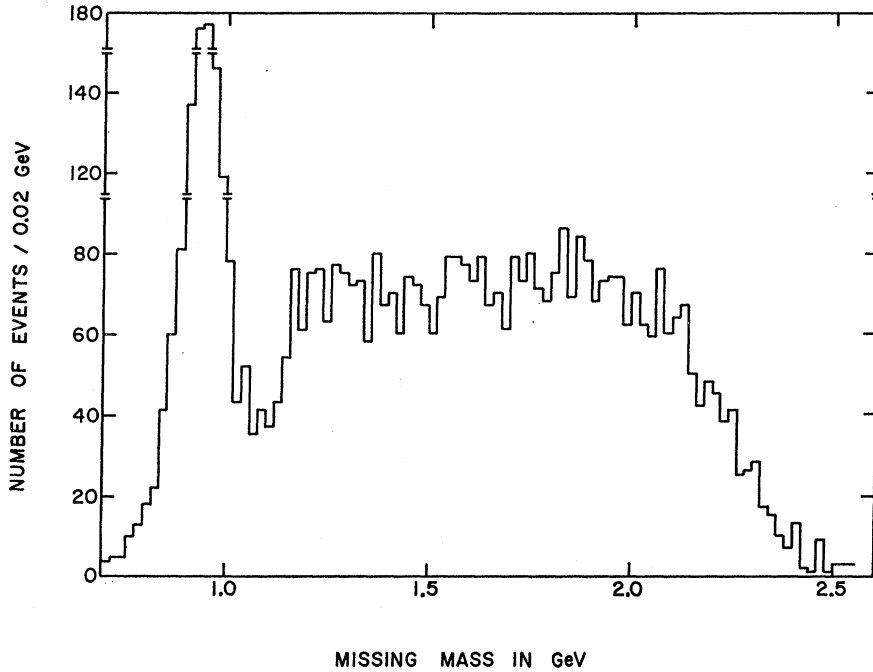
FIG. 3. Missing mass from the reaction $K^-d \to \bar{K}^0\pi^- p\mathrm{MM}$ (5311 events.)
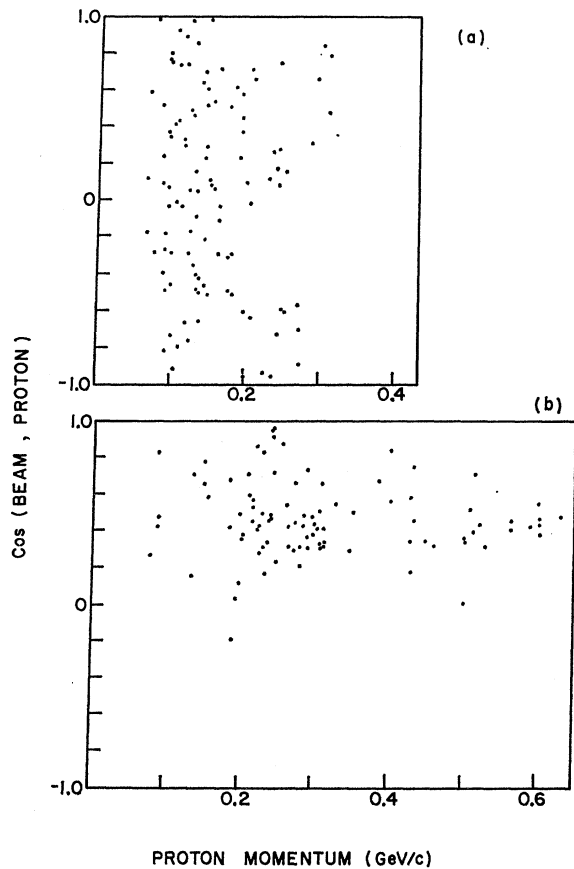

FIG. 4. Cosine of the angle between the beam and the outgoing proton plotted against the proton momentum: (a) $p_p < p_n$; (b) $p_p > p_n$.

with events identified as reaction (2) removed. Events were accepted as neutron fits if the missing mass was less than 1.1 GeV and the confidence level for reaction (1) was greater than 1%.

According to the impulse approximation model,[8] the final state

$$K^-d \to \bar{K}^0\pi^- np \tag{1}$$

can be categorized as a K^-p or K^-n interaction with the other nucleon merely acting as a spectator. The lower-momentum nucleon was assumed to be the spectator in the reaction. This assumption was investigated by looking at those events in which the $K^*(890)$ resonance was produced. Let $\cos\theta$ be the cosine of the angle between the nucleon in question and the incident beam in the laboratory reference system. The spectator nucleons are expected to have an isotropic $\cos\theta$ distribution but for interaction nucleons the situation is quite different. If the nucleon were at rest in the laboratory, it would be kinematically impossible for the nucleon to go off in the backward direction. We generated Monte Carlo events in which we assumed a target momentum distribution as determined by the Hulthén distribution and the observed momentum-transfer distribution to the $K^*(890)$. We found that we should expect, at most, 10% of all interaction nucleons to lie in the backward hemisphere for $K^*(890)$ production.

In Fig. 4(a) (5(a)), $\cos\theta$ is plotted against the proton (neutron) momentum for events in which the proton

[8] L. Hulthén and M. Sugawara, in *Handbuch der Physik*, edited by S. Flügge (Springer-Verlag, Berlin, 1957), Vol. 39, p. 1. We are studying departures from the Hulthén distribution [J. Tebes *et al.* (unpublished)].

(neutron) has the smaller momentum. In both cases, the lower-momentum nucleon evenly populates the forward and backward hemispheres. Figure 4(b) (5(b)) shows $\cos\theta$ plotted against the proton (neutron) momentum for events in which the proton (neutron) has the larger momentum. As can be seen, almost all events populate the forward hemisphere. We conclude that the choice of the lower-momentum nucleon as the spectator was correct statistically. We also required that the spectator have a laboratory momentum less than 0.3 GeV/c.

For reaction (3), the classification is less unambiguous. This reaction leads to a one-constraint fit at the primary vertex and is more easily faked. Since the corresponding neutron-proton reaction

$$K^- d \rightarrow \bar{K}^0 \pi^- \pi^0 pn \tag{7}$$

is not analyzable, the tests used to select the deuteron in reaction (2) could not be used. Furthermore, curvature information was not available because of the short length of the deuteron tracks. The square of the missing mass (MM^2) from the reaction

$$K^- d \rightarrow K^0 \pi^- d\text{MM} \tag{8}$$

for events which fit reaction (3) with a 1% or better

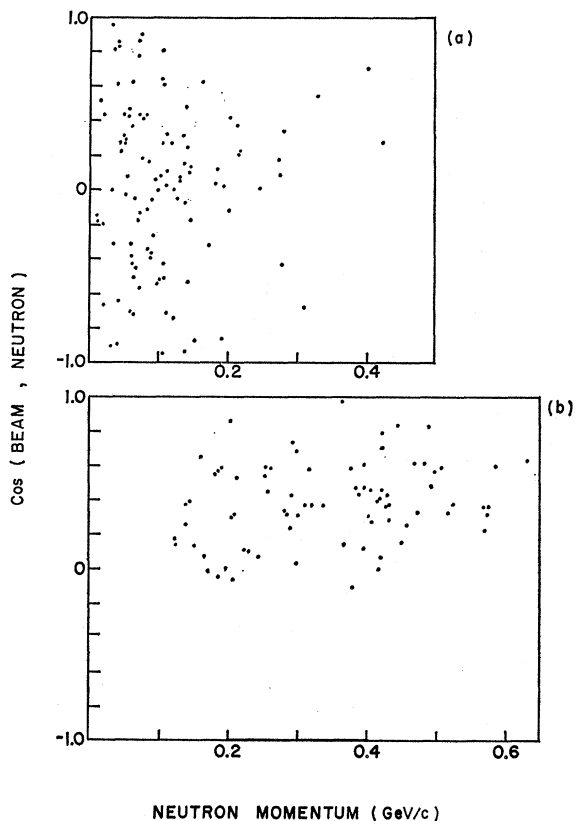**NEUTRON MOMENTUM (GeV/c)**

FIG. 5. Cosine of the angle between the beam and the outgoing neutron plotted against the neutron momentum: (a) $p_n < p_p$; (b) $p_n > p_p$.
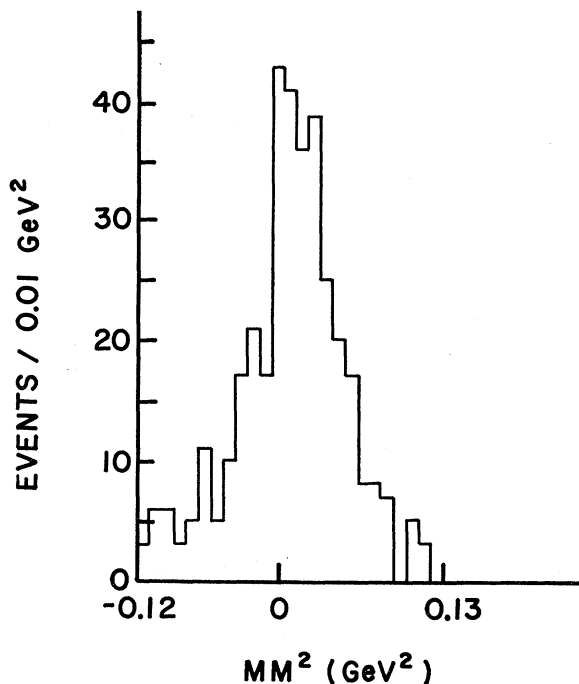
FIG. 6. Missing-mass-squared distribution from the reaction $K^- d \rightarrow \bar{K}^0 \pi^- d\text{MM}$, for events which fit $K^- d \rightarrow \bar{K}^0 \pi^- \pi^0 d$ with a 1% probability.

probability is given in Fig. 6. The peak at the position of the square of the π^0 mass is an indication that we actually have reaction (3) events. We required that the missing mass squared lie between -0.03 and 0.07 GeV^2 for an event to be interpreted as reaction (3).

Using the above criteria we estimate that the percentages of misassigned events are 10, 5, and at least 20% for reactions (1), (2), and (3), respectively. The misassignment in events has been taken into account in the cross-section determination. A summary of the number of events accepted in each reaction is shown in Table I.

The cross section has been corrected for scanning efficiency, beam purity, $\bar{K}^0$ branching ratio, losses due to failures in the reconstruction program, and detection efficiency for $\bar{K}_1^0$'s. For the $K^- n$ events, the Glauber screening effect[9] has also been taken into account.

TABLE I. Events assigned to each reaction.

Reaction	Number of events	Cross section (mb)
$K^- d \rightarrow p_s \bar{K}^0 \pi^- n$	1321	0.758±0.021
$\rightarrow d\bar{K}^0 \pi^-$	83	0.048±0.005
$\rightarrow d\bar{K}^0 \pi^- \pi^0$	246	0.141±0.009
$\rightarrow p_s \bar{K}^0 \pi^- \text{MM}$	4074	2.340±0.036

[9] R. J. Glauber, Phys. Rev. **100**, 242 (1965); W. Galbraith, E. W. Jenkins, T. F. Kycia, B. A. Leontic, R. H. Phillips, A. L. Read, and R. Rubinstein, *ibid.* **138**, B913 (1965).

III. FINAL STATE $K^-d \to \bar{K}^0\pi^-np$

We will be concerned with analyzing the

$$K^-n \to \bar{K}^0\pi^-n \qquad (9)$$

final state, since the reaction

$$K^-p \to \bar{K}^0\pi^-p \qquad (10)$$

is better studied in a hydrogen-filled bubble chamber.

A. General Features

Figure 7 shows the Dalitz plot of $M^2(\pi^-n)$ versus $M^2(\bar{K}^0\pi^-)$ for reaction (9). Strong $K^{*-}(890)$ and $\Delta^-(1236)$ production is evident. In addition there is evidence for $K^{*-}(1420)$ production but a large $K^*(1420)$ $-\Delta(1236)$ overlap is not observed.[10] This is in contrast to the Brussels-CERN collaboration's[11] investigation of the reaction $K^+p \to K^0\pi^+p$ at 3.5 GeV/c where a
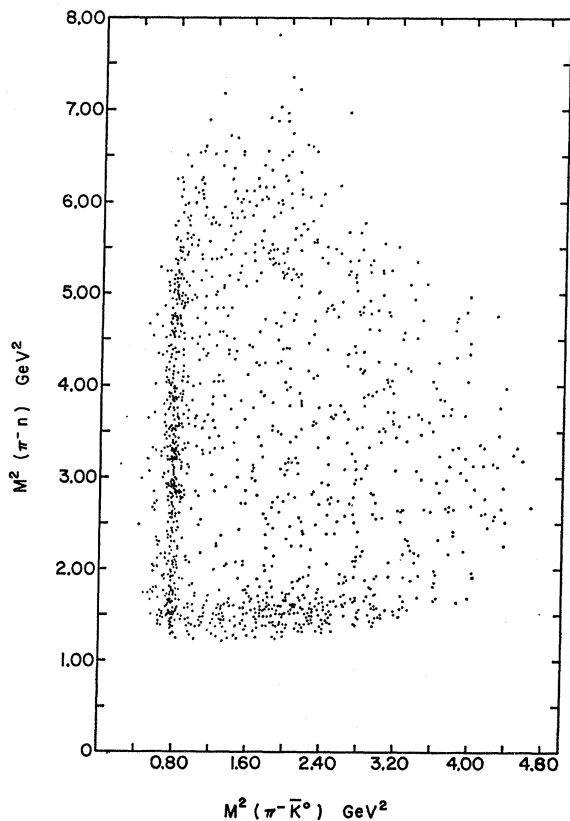

FIG. 7. Dalitz plot of $M^2(\pi^-n)$ versus $M^2(\bar{K}^0\pi^-)$ for the events fitting $K^-d \to p_s\bar{K}^0\pi^-n$.

[10] We define the $K^*(1400)$ region as $1.37 \leq M(K^0\pi^-) \leq 1.47$ GeV. The $\Delta(1236)$ band is taken as $1.17 \leq M(\pi^-n) \leq 1.31$ GeV. There are 29 events in the overlap band out of a total of 124 events in the entire $K^*(1400)$ region.

[11] W. De Baere, J. Debaisieux, P. Dufour, F. Grard, J. Heughebaret, L. Pape, P. Peters, F. Verbeure, R. Windmolders, Y. Goldschmidt-Clermont, V. P. Henri, B. Jongejans, A. Moisseev, F. Muller, J. M. Perreau, A. Prokes, and V. Yarba, Nuovo mento **51A**, 401 (1967).

large constructive interference between the $\Delta^{++}(1236)$ and the $K^*(1420)$ is found. A similar type of energy-dependent interference is also seen in $K^*(890) - \Delta(1236)$ production[12] where at low energies there is strong constructive interference of the two amplitudes which disappears as the energy of the reaction increases.

Figure 8 shows the $\bar{K}^0\pi^-$, π^-n, and $\bar{K}^0n$ effective-mass distributions. In addition to $K^*(890)$, $K^*(1420)$, and $\Delta(1236)$, the $\bar{K}^0n$ mass projection shows the production of $\Lambda(1520)$ and a broad enhancement at ~ 1.85 GeV.

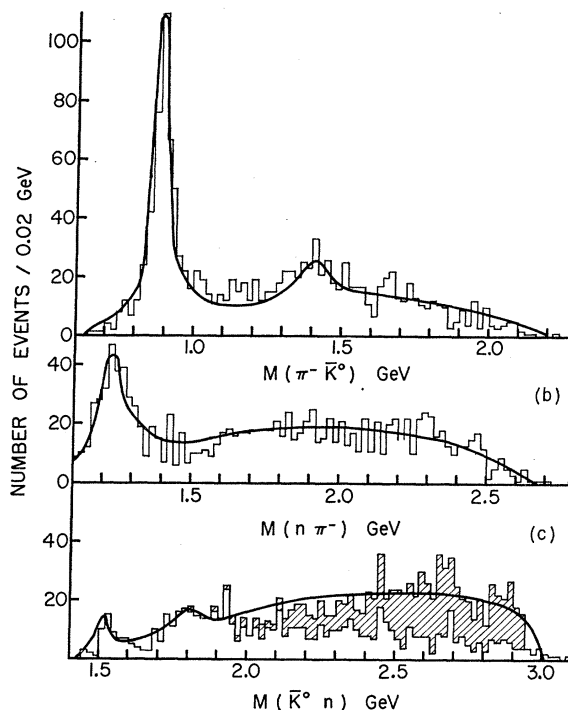The relative fraction of resonance production was calculated using the maximum likelihood program

FIG. 8. Effective-mass distributions for the reaction $K^-d \to p_s\bar{K}^0\pi^-n$: (a) $M(\bar{K}^0\pi^-)$; (b) $M(\pi^-n)$; (c) $M(\bar{K}^0n)$. The shaded area in (c) corresponds to $\Delta(1236)$ or $K^*(890)$ events.

MURTLEBERT.[13] The masses and widths of the resonances were input to the fit and the proper variation of the center-of-mass energy was included. Table II gives the fractional contributions from each resonance. The mass and width of the resonances used in the fit are also given. The solid curves in Fig. 8 represent a Monte Carlo sample generated using the results of the fit.

We note that the relative ratio of $\Delta(1236)$ to $K^*(890)$ production is much smaller than that found in the

[12] R. W. Bland, M. G. Bowler, J. L. Brown, G. Goldhaber, S. Goldhaber, J. A. Kadyk, and G. H. Trilling, Phys. Rev. Letters **17**, 939 (1965).

[13] Jerry Friedman, Alvarez Programming Group Report No. p-156, 1966 (unpublished). The original Berkeley program was revised by R. Miller; see Purdue High Energy Physics Report No. 3.1, 1968 (unpublished).

K^+p 3.5-GeV/c experiment,[11] in which a ratio of about one to one was reported.

Recently, several resonances in the $K\pi$ mass spectrum between the well-known $K^*(890)$ and $K^*(1420)$ were reported. They are $K^*(1080)$,[11] $K^*(1160)$,[14] and $K^*(1260)$.[15] We do not observe any statistically significant $\bar{K}^0\pi^-$ mass peaks in this mass range. (See, however, Sec. III F for a discussion of the asymmetry and moments in the $\bar{K}^0\pi^-$ system.)

Figures 9(a) and 9(b) show the $\bar{K}^0\pi^-$ and π^-p effective-mass distribution of the hydrogenlike events of reaction (10). This sample of 253 events which is strongly biased toward low-momentum protons is dominated by $K^*(890)$ production. There is little evidence for any $\Delta(1236)^0$ production. As a further test that we have separated the neutron and proton spectators with a high degree of efficiency, we have looked at the π^-n_s effective-mass spectrum [Fig. 9(c)] and

TABLE II. Processes contributing to $\pi^-\bar{K}^0n$ final state.

Process	Fraction	Cross section (μb)
$K^-n \to nK^{*-}(892,49)$	0.311 ± 0.016	236 ± 12
$\searrow \pi^-\bar{K}^0$		
$nK^{*-}(1420,90)$	0.060 ± 0.014	46 ± 11
$\searrow \pi^-\bar{K}^0$		
$\bar{K}^0\Delta^-(1236,120)$	0.213 ± 0.016	162 ± 12
$\searrow \pi^-n$		
$\pi^-\Lambda(1518,16)$	0.015 ± 0.005	11 ± 4
$\searrow \bar{K}^0n$		
$\pi^-\Lambda(1815,75)$	0.040 ± 0.011	30 ± 8
$\searrow \bar{K}^0n$		
$\pi^-\Lambda(2670,50)$	0.004 ± 0.009	3 ± 7
$\searrow \bar{K}^0n$		
$\pi^-\bar{K}^0n$ (phase space)	0.357	271

found no evidence for $\Delta^-(1236)$ production. Since a large sample of K^-p interactions at 3, 9, 4.6, and 5.0 GeV/c incident momenta is available from a BNL 80-in. hydrogen-bubble-chamber exposure, we shall compare our K^-n interactions to it.[5]

B. Production and Decay of $K^{*-}(890)$

Reaction (9) is dominated by $K^*(890)$ production[16] (31%). The four-momentum transfer squared $-t$ between the incident K^- and the outgoing $\bar{K}^0\pi^-$ is plotted as a function of the $\bar{K}^0\pi^-$ mass squared in Fig. 10. The Chew-Low plot indicates a peripheral production mechanism. Backward K^* production could

[14] D. J. Crennell, U. Karshon, K. W. Lai, J. S. O'Neall, and J. M. Scarr, Phys. Rev. Letters **22**, 487 (1969).

[15] W. P. Dodd, T. Joldersma, R. B. Palmer, and N. P. Samios, Phys. Rev. **177**, 1991 (1969).

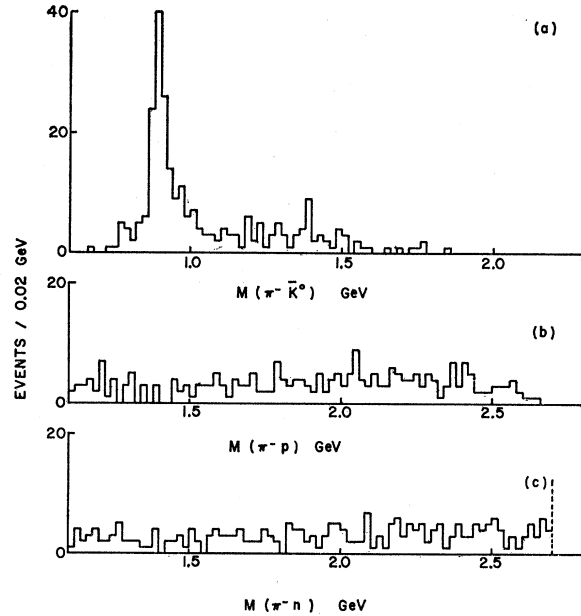[16] The $K^*(890)$ resonance region is defined as $0.83 \leq M(K^0\pi^-) \leq 0.96$ GeV.

FIG. 9. Effective-mass distributions for the reaction $K^-d \to n_s\bar{K}^0\pi^-p$: (a) $M(\bar{K}^0\pi^-)$; (b) $M(\pi^-p)$; (c) $M(\pi^-n)$.

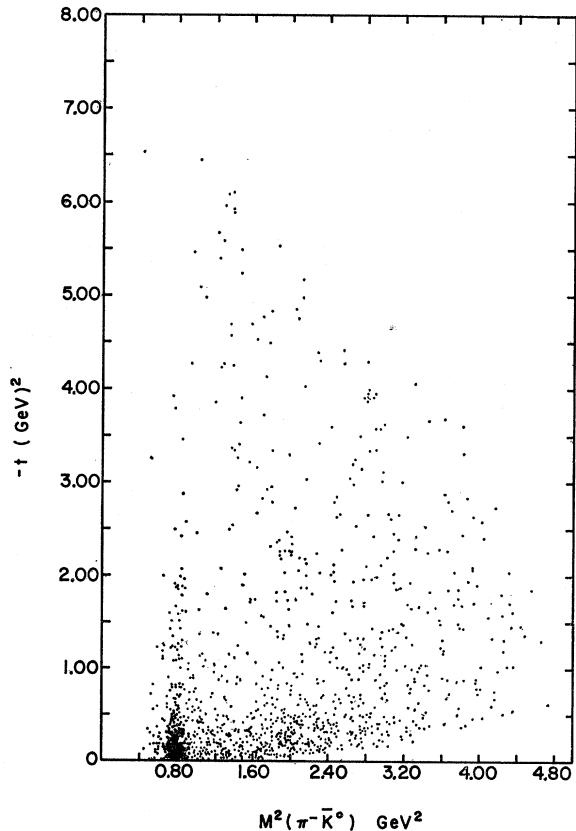
FIG. 10. Chew-Low plot for the reaction $K^-n \to \bar{K}^0\pi^-n$. (1321 events.)
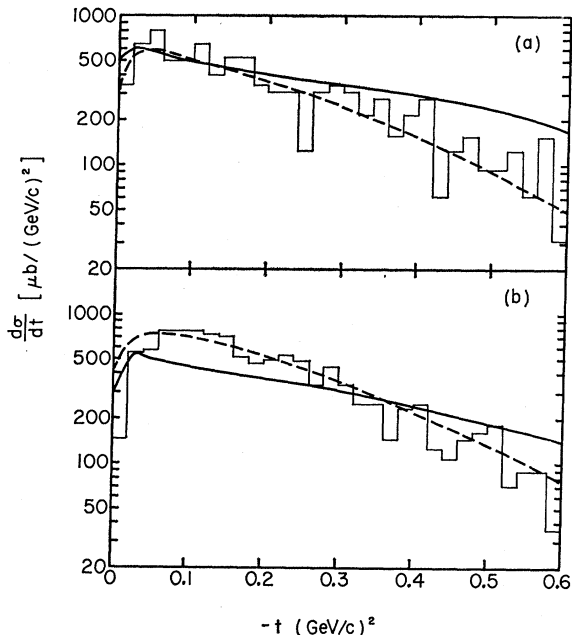
FIG. 11. Production angular distribution for the $K^*(890)$. Absorption-model predictions are shown as solid curves. The Regge-pole-model predictions are shown dashed. (a) $K^-n \to K^{*-}(890)n$; (b) $K^-p \to K^{*-}(890)p$.

be mediated by an exchange of a positive strangeness baryon. In agreement with K^-p results at 4.1,[17] 5.5,[17] and 10.1 GeV/c,[18] we found no evidence for backward $K^*(890)$ production.

The production angular distribution of the $K^*(890)$ as a function of four-momentum transfer squared is given in Fig. 11(a). A least-squares fit to the distribution was performed using an exponential form

$$\frac{d\sigma}{dt} = Ae^{Bt}. \qquad (11)$$

For the region $0.1 \leq -t \leq 0.5$ (GeV/c)^2, we found $A = 831 \pm 158\,\mu$b (GeV/c)$^{-2}$ and $B = 3.9 \pm 0.6$ (GeV/c)$^{-2}$. The same parametrization [Fig. 11(b)] of the Brookhaven hydrogen data gave $A = 1295 \pm 161\,\mu$b (GeV/c)$^{-2}$ and $B = 4.2 \pm 0.5$ (GeV/c)$^{-2}$. The differential cross section has a maximum at $|t| \sim 0.06$ (GeV/c)^2. A similar "bending over" in the vicinity of $t=0$ has also been observed at 4.1,[17] 4.57,[19] 5.5,[17] 6.0,[20] and 10.1[18] GeV/c for the reaction $K^-p \to pK^{*-}(890)$.

The $K^*(890)$ decay angular distribution may be written in terms of its spin-space density-matrix ele-

---

ments $\rho_{mm'}$ as

$$W(\cos\theta,\varphi) = (\tfrac{3}{4}\pi)[\tfrac{1}{2}(1-\rho_{00}) + \tfrac{1}{2}(3\rho_{00}-1)\cos^2\theta$$
$$-\rho_{1-1}\sin^2\theta\cos2\varphi - \sqrt{2}\,\mathrm{Re}\rho_{10}\sin2\theta\cos\varphi], \qquad (12)$$

where θ and φ are the polar and azimuthal angles of the decay $\bar{K}^0$ in the $K^*(890)$ rest frame (Jackson frame[21]), the z axis being taken as the direction of the incident K^- and the y axis as the direction of the normal to the production plane. Integrating over φ and $\cos\theta$, respectively, gives

$$W(\cos\theta) = \tfrac{3}{4}[(1-\rho_{00}) + (3\rho_{00}-1)\cos^2\theta] \qquad (13)$$

and

$$W(\varphi) = (\tfrac{1}{2}\pi)\{(1+2\rho_{1-1}) - 4\rho_{1-1}\cos^2\varphi\}. \qquad (14)$$

To avoid any biases that may influence the K^* angular distribution from the overlap of the $\Delta(1236)$ band we have followed a suggestion by Eberhard and Pripstein[22] and have repopulated the overlap region with "conjugate events." It was found, however, that the analysis presented below gave the same results with or without the repopulation of the overlap region.

The method of moments was used to evaluate the $K^*(890)$ density-matrix elements. They are plotted in Figs. 12(a)–12(c) for K^-n interactions and in Figs.
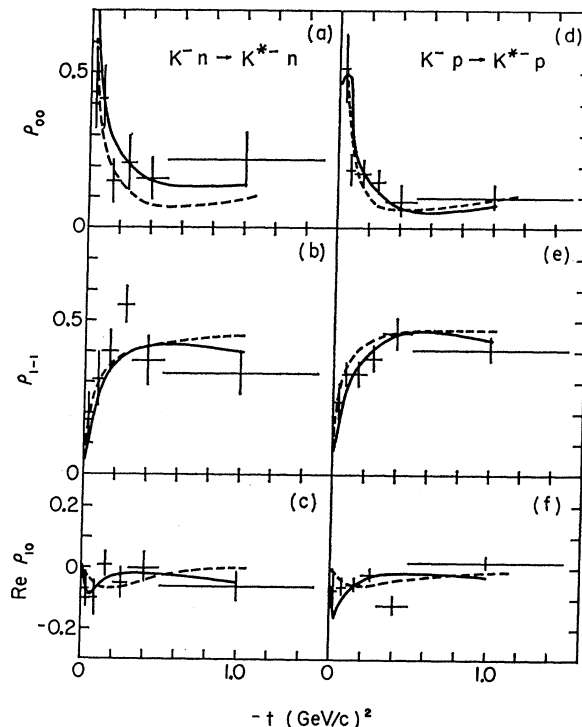

FIG. 12. Density-matrix elements for the $K^*(890)^-$. Absorption-model predictions are shown as solid curves and Regge-model predictions as dashed. (a)–(c) $K^-n \to K^*(890)n$; (d)–(f) $K^-p \to K^*(890)p$.

[17] F. Schweingruber, M. Derrick, T. Fields, D. Griffiths, L. G. Hyman, R. J. Jabbur, J. Loken, R. Ammar, R. E. P. Davis, W. Kropac, and J. Mott, Phys. Rev. **166**, 1317 (1968).

[18] Aachen-Berlin-CERN-London (I. C.)-Vienna Collaboration, M. Aderholz *et al.*, Nucl. Phys. **B5**, 567 (1968).

[19] Y. W. Kang, Phys. Rev. **176**, 1587 (1968).

[20] Birmingham-Glasgow-London (I.C.)-München-Oxford-Rutherford Collaboration, D. C. Colley *et al.*, Nuovo Cimento **53A**, 522 (1968).

[21] J. D. Jackson, Rev. Mod. Phys. **37**, 484 (1965).

[22] P. Eberhard and M. Pripstein, Phys. Rev. Letters **10**, 351 (1963).

12(d)–12(f) for K^-p interactions and are tabulated in Table III. The $\cos\theta$ and φ projections of the decay angular distributions for the K^-n events are shown in Fig. 13.

As the comparison of $K^*(890)$ production in K^-n and K^-p interactions has already been reported elsewhere,[5] we shall only summarize the main results.

The density matrices are very similar for both reactions; in particular, the ρ_{00} matrix element rises rapidly in the same four-momentum transfer region as the forward dip in the differential cross section. In the context of the absorption model,[21] there are two free parameters λ and γ given by

$$\lambda = f_{VK^*K}(G^V + G^T)/2f_{\pi K^*K}g_{\pi NN} \qquad (15)$$

and

$$\gamma = 2G^T/(G^T + G^V), \qquad (16)$$

where, f, g, and G are coupling constants as defined by Jackson and Pilkuhn.[23] The best parameters found are $\lambda = \pm 0.9 \pm 0.2$ and $\gamma = 0.6 \pm 0.2$, where λ is $+$ $(-)$ for K^-p (K^-n) interactions, respectively. The solid curves in Figs. 11 and 12 are the absorption model predictions corresponding to the best values of λ and γ. There is general agreement with the data except that the predictions for $d\sigma/dt$ are not reliable for momentum transfer above about $-t = 0.4$ $(\text{GeV}/c)^2$. The parameters (λ, γ) are supposedly constants; however, they are found to be $(1.8, 1.15)$, $(1.55, 0.95)$, $(0.81, 0.6)$, $(0.9, 0.6)$, $(0.6, 0.0)$, and $(0.4, 0.2)$ at 2.64, 3.0, 3.5, 4.5, 6.0, and 10.1 GeV/c, respectively.[24]

In a recent paper, Donohue[25] suggested that the production and decay angular distribution of the $K^*(890)$ in K^-n and K^-p interactions might exhibit different behaviors at small momentum transfers since the sign of the interference term between pion and ω exchange would be different. The only difference we have seen in these two reactions is that the K^-n distributions have a smaller forward dip in the differential

FIG. 13. $\cos\theta$ and φ decay distributions for the $K^{*-}(890)$ in reaction (9). The solid curves are calculated from the density-matrix elements. The dashed events are repopulated events. From top to bottom the $|t|$ intervals are 0–0.05, 0.05–0.1, 0.1–0.2, 0.2–0.3, 0.3–0.5, and 0.5–1.5 $(\text{GeV}/c)^2$.

cross section than the K^-p; that is, in the region $0.02 < -t < 0.1$ $(\text{GeV}/c)^2$, the slope of $\ln(d\sigma/dt)$ is 6.5 ± 4.7 $(\text{GeV}/c)^{-2}$ for the K^-n data and -6.3 ± 3.4 $(\text{GeV}/c)^{-2}$ for the Kp. The predicted differences in the density-matrix elements are too small to be checked with the present data.

A comparison to the Regge-pole model of Dass and Froggatt[26] was also made. The Regge predictions (Figs. 11 and 12) are good over the entire momentum-transfer region and predict the correct energy dependence of the $K^*(890)$ cross section. The extent to which the improved fit is due to the increased physical content of the Regge-pole model rather than the increased number of parameters is not entirely clear.

C. Production and Decay of $\Delta^-(1236)$

The production of the $\Delta(1236)$ resonance[10] contributes 21% to reaction (9). In the rest frame of the $\Delta(1236)$, we define the z axis along the direction of the target nucleon, and the y axis as the normal to the production plane. The decay distribution for the $\Delta(1236)$ can be expressed in terms of its spin-density-matrix

TABLE III. Comparison of K^{*-} density-matrix elements in K^-n and K^-p interactions at 4.5 GeV/c.

$-t$ $(\text{GeV}/c)^2$		N (events)	ρ_{00}	$\text{Re}\rho_{1,-1}$	$\text{Re}\rho_{10}$
0.0 −0.05	K^-n	46	0.44±0.12	0.18±0.08	−0.07±0.06
	K^-p	63	0.52±0.11	0.24±0.06	−0.07±0.05
0.05−0.1	K^-n	40	0.42±0.11	0.31±0.09	−0.10±0.06
	K^-p	94	0.19±0.05	0.33±0.04	−0.06±0.03
0.1 −0.2	K^-n	79	0.15±0.07	0.40±0.07	0.01±0.04
	K^-p	179	0.18±0.04	0.33±0.04	−0.05±0.02
0.2 −0.3	K^-n	46	0.21±0.09	0.55±0.06	−0.05±0.05
	K^-p	128	0.15±0.04	0.38±0.04	−0.02±0.02
0.3 −0.5	K^-n	60	0.16±0.07	0.37±0.08	0.00±0.05
	K^-p	113	0.09±0.05	0.46±0.05	−0.12±0.03
0.5 −1.5	K^-n	61	0.22±0.09	0.33±0.07	−0.06±0.05
	K^-p	120	0.10±0.04	0.41±0.04	0.02±0.02

[23] J. D. Jackson and H. Pilkuhn, Nuovo Cimento **33**, 906 (1964); **34**, 1841(E) (1964).

[24] These values, except the ones from our data, are taken from the quoted values in Ref. 18.
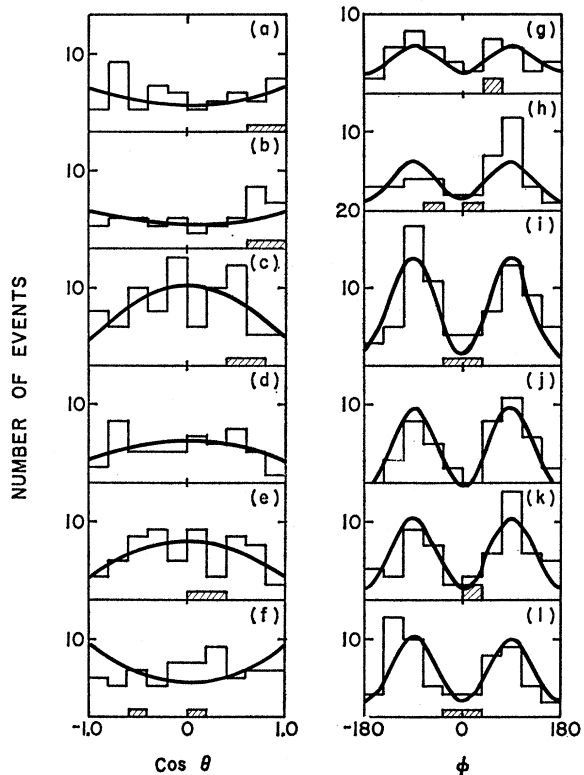
[25] J. T. Donohue, Phys. Rev. **163**, 1549 (1967).

[26] G. V. Dass and C. D. Froggatt, Nucl. Phys. **B10**, 151 (1969). The curves presented here are a slight modification of the curves which we used in our Ref. 5. We thank Dr. Dass for this private communication.
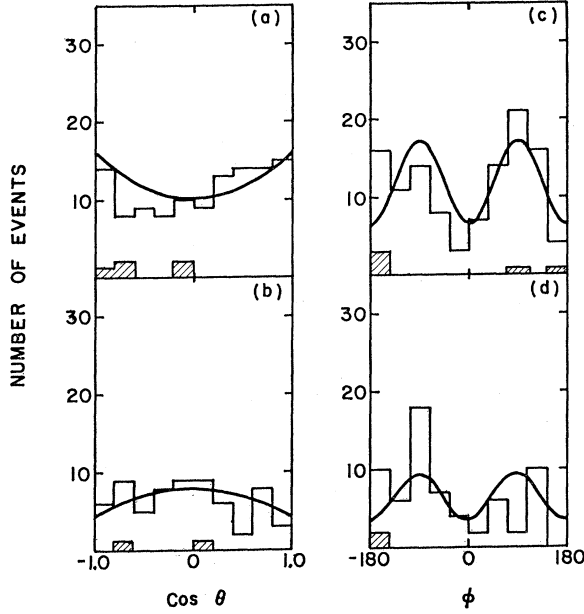
FIG. 14. $\cos\theta$ and φ decay distributions for the $\Delta(1236)^-$ in the reaction $K^-n \to \bar{K}^0\Delta^-(1236)$. The solid curves are calculated from the density-matrix elements. The dashed events are repopulated events. The upper histograms are for $|t| < 0.25$; the lower for $0.25 < |t| < 0.8$ $(\text{GeV}/c)^2$.

elements $\rho_{2m,2m'}$ as

$$W(\cos\theta,\varphi) = (3/4\pi)[\tfrac{1}{6}(1+4\rho_{33})+\tfrac{1}{2}(1-4\rho_{33})\cos^2\theta$$
$$- (2/\sqrt{3})\,\text{Re}\rho_{3-1}\sin^2\theta\,\cos2\varphi$$
$$- (2/\sqrt{3})\,\text{Re}\rho_{31}\sin2\theta\,\cos\varphi]. \quad (17)$$

The $\cos\theta$ and φ projections are

$$W(\cos\theta) = \tfrac{1}{4}[(1+4\rho_{33})+(3-12\rho_{33})\cos^2\theta] \quad (18)$$

and

$$W(\varphi) = (1/2\pi)[1+(4/\sqrt{3})\,\text{Re}\rho_{3-1}$$
$$- (8/\sqrt{3})\,\text{Re}\rho_{3-1}\cos^2\varphi]. \quad (19)$$

In accordance with the prescription described in the analysis of $K^*(890)$, we repopulated the overlap Δ-K^* band with events in the conjugate region. Figure 14 shows the $\cos\theta$ and φ projections. The solid curves were calculated from the values of the density-matrix elements obtained by using the method of moments. The density-matrix elements are given in Table IV. On the basis of parity and G-parity conservation,

TABLE IV. $\Delta(1236)$ density-matrix elements for the reaction $K^-n \to \Delta^-(1236)\bar{K}^0$.

$-t$ $(\text{GeV}/c)^2$	N	ρ_{33}	$\text{Re}\rho_{3-1}$	$\text{Re}\rho_{31}$
0.0 −0.25	119	0.165±0.054	0.194±0.048	0.109±0.045
0.25−0.8	67	0.340±0.063	0.196±0.071	−0.087±0.058
>0.8	48	0.481±0.059	−0.011±0.098	0.023±0.070

Thews[27] has developed general relationships among density-matrix elements that allow one to decide if more than one particle (or trajectory) contributes to a given reaction (if cuts and/or absorption effects can be neglected). For the process

$$K^-n \to \bar{K}^0\Delta^-(1236), \quad (20)$$

the relation

$$(\tfrac{1}{2}-\rho_{33})\rho_{33} = (\text{Re}\rho_{31})^2+(\text{Re}\rho_{3-1})^2 \quad (21)$$

must be satisfied if only one trajectory contributes. We find the difference between the left- and right-hand sides of (21) to be

$$0.006\pm0.024 \quad \text{for} \quad 0\le -t\le 0.25 \ (\text{GeV}/c)^2$$

and

$$0.007\pm0.028 \quad \text{for} \quad 0.25\le -t\le 0.80 \ (\text{GeV}/c)^2,$$

and thus no conclusions can be reached on the number of exchanged particles contributing to (20). It has been suggested by Thews[27] and Maor and Krammer[28] that both the ρ and A_2 Regge trajectories contribute to Δ^{++} production in

$$K^+p \to K^0\Delta^{++}(1236). \quad (22)$$

The A_2 trajectory is expected to go through zero in the neighborhood of $-t=0.5$ $(\text{GeV}/c)^2$ and could produce a dip in the differential cross section for $\Delta^-(1236)$ production (Fig. 15). No dip near $-t=0.5$ $(\text{GeV}/c)^2$ is found in agreement with the K^+p results[29] at 3.5 and 5.0 GeV/c. We have fitted the differential cross section to the form $d\sigma/dt = Ae^{Bt}$ and found $A=483\pm110$ μb $(\text{GeV}/c)^{-2}$ and $B=4.0\pm0.7$ $(\text{GeV}/c)^{-2}$ over the mo-
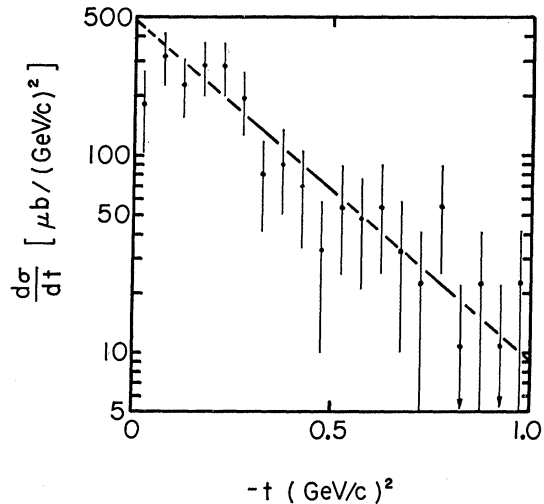

FIG. 15. $\Delta(1236)$ production differential cross section in the reaction $K^-n \to \bar{K}^0\Delta^-(1236)$.

[27] R. L. Thews, Phys. Rev. **155**, 1624 (1967); G. A. Ringland and R. L. Thews, *ibid.* **170**, 1569 (1968).
[28] M. Krammer and U. Maor, Nuovo Cimento **52A**, 308 (1967).
[29] D. C. Colley, in *Proceedings of the Topical Conference on High Energy Collisions of Hadrons* (CERN, Geneva, 1968), Vol. 1, p. 60.

mentum-transfer region $0.5 \leq -t \leq 0.70$ $(\mathrm{GeV}/c)^2$. The exponent agrees with the K^+p results at 3.5 and 5.0 GeV/c, namely, 3.5 ± 0.5 and 4.1 ± 0.7 $(\mathrm{GeV}/c)^{-2}$, respectively.

D. Production of $K^*(1420)$

The $K^*(1420)$ is produced with a substantial amount ($\sim 46\%$) of nonresonant background. Figure 16 shows the production angular distribution for the $K^*(1420)$ events. $K^*(1420)$ is produced peripherally. No appreciable contribution is seen in the backward direction in agreement with production by single-meson exchange.

E. Production of $\Lambda(1520)$

As is seen in Fig. 8(c), a small amount (1.5%) of $\Lambda(1520)$ is also produced in reaction (9) and does not kinematically overlap $\Delta(1236)$ or $K^*(890)$ production. The production angle between the incident K^- and the outgoing π^- in the over-all center-of-mass system of reaction (9) is shown in Fig. 17(a) for the $\Lambda(1520)$ events. This resonance can be produced in the forward direction by the exchange of a vector meson (K^*) and in the backward direction by baryon exchange. The observed backward production is indicative of a strong $Kp\Lambda(1520)$ vertex. In Figs. 17(b) and 17(c), we show the analogous distributions at 3.0 GeV/c [30] and 5.5 GeV/c.[31]

F. Asymmetry and Moments across $\bar{K}^0\pi^-$ Mass Spectrum

We define θ as the scattering angle between the incident K^- and the outgoing $\bar{K}^0$ in the $\bar{K}^0\pi^-$ rest frame in the reaction $K^-n \to \bar{K}^0\pi^-n$. Figure 18 shows a scatter plot of $\cos\theta$ as a function of the $K\pi$ effective mass. The asymmetry parameter α is defined by

$$\alpha = (F-B)/(F+B), \tag{23}$$

where F and B are the numbers of events in the forward

FIG. 17. $\Lambda(1520)$ production angular distribution (a) $K^-n \to \pi^-\Lambda(1520)$ with $\Lambda(1520) \to \bar{K}^0n$ at 4.5 GeV/c; (b) $K^-n \to \pi^-\Lambda(1520)$ with $\Lambda(1520) \to \bar{K}N$, $\Sigma\pi$ at 3.0 GeV/c; (c) $K^-p \to \pi^-\Lambda(1520)$ with $\Lambda(1520) \to \Sigma\pi$ at 5.5 GeV/c.

and backward hemispheres, respectively. Figure 19 presents the forward-backward asymmetry parameter as a function of the $K\pi$ effective mass both for all the data and for the events with the $\Delta(1236)$ removed. The removal of the sizable $\Delta(1236)$ contribution does not alter the asymmetry parameters significantly and in the subsequent analysis of the moments these events were excluded. The asymmetry parameter changes from
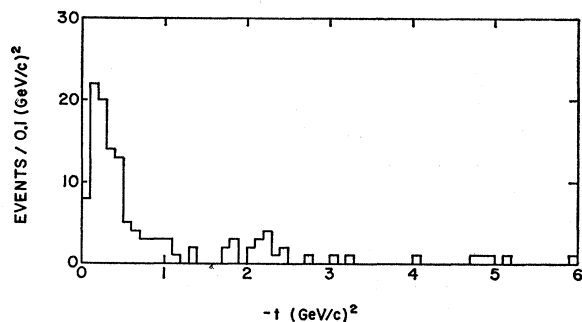

FIG. 16. Production distribution for the $K^*(1420)$ events in the reaction $K^-n \to \bar{K}^0\pi^-n$.

[30] S.A.B.R.E. Collaboration, J. C. Scheuer et al., Nucl. Phys. **B8**, 503 (1968).

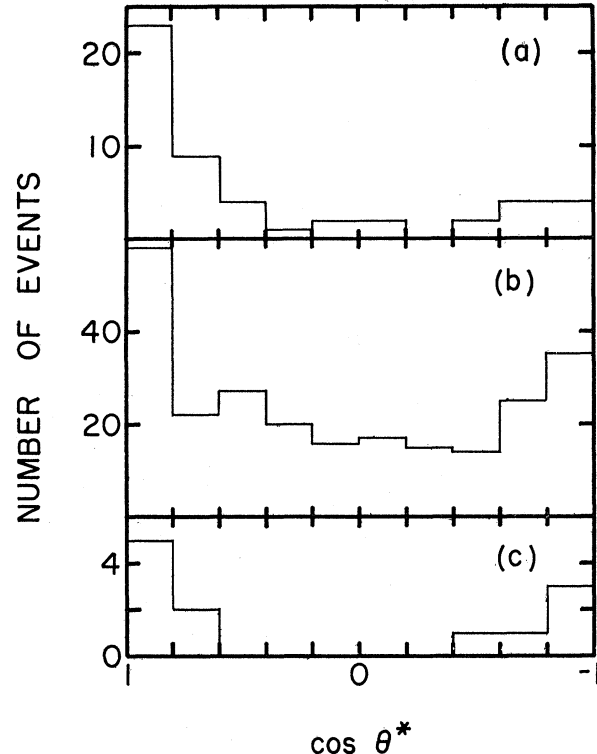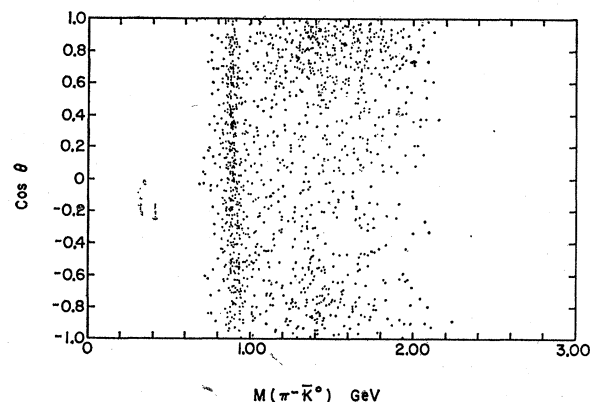[31] U. E. Kruse, J. S. Loos, and E. L. Goldwasser, Phys. Rev. **177**, 1951 (1969).

FIG. 18. $\cos\theta$, the K scattering angle (see text), as a function of the $\bar{K}^0\pi^-$ effective mass from the reaction $K^-n \to \bar{K}^0\pi^-n$.
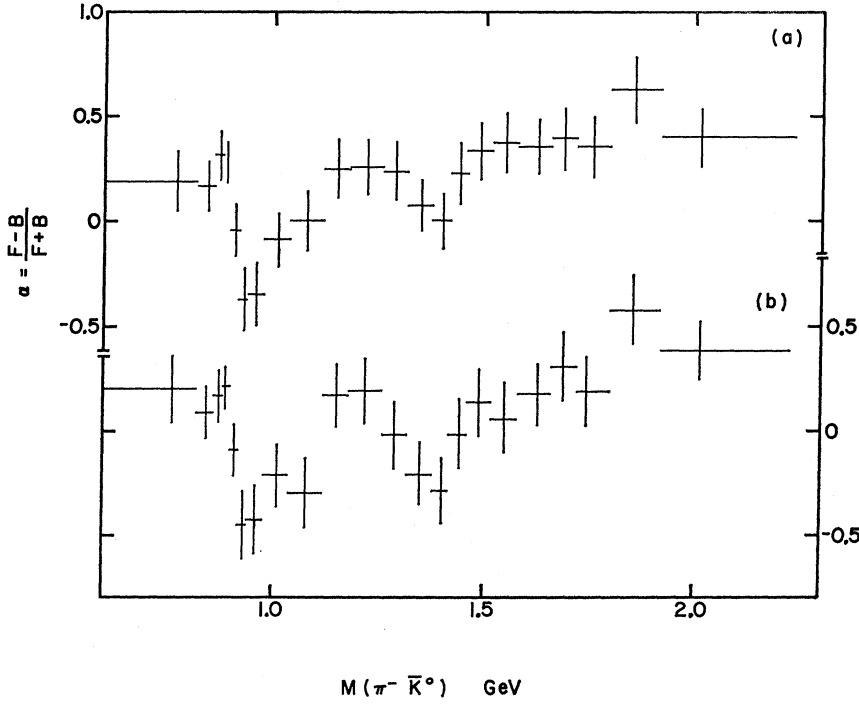
FIG. 19. Forward-backward asymmetry as a function of $M(\bar{K}^0\pi^-)$. (a) Total sample; (b) $\Delta(1236)^-$ events removed.

positive to negative near 0.9 GeV/c^2 and then becomes positive again at 1.1 GeV/c^2. This behavior suggests the intriguing possibility that there may be another resonance in this region which interfers with the p-wave to give the observed asymmetry. We have analyzed the kaon-boson scattering in the $K\pi$ rest frame in terms of moments Y_l^m. The z axis of our coordinate system was chosen along the incident K^- direction and the y axis

along the production normal.[32] In Fig. 20, we have plotted all the possible expectation values of ReY_l^m up to $l=4$. The interpretation of the analysis of $K\pi$ scattering is more difficult than that of $\pi\pi$ scattering in πN reactions because of the sizable amount of vector (assumed ω) exchange involved. We may, however, write the differential cross section[33] for the reaction $K^-n \to \bar{K}^0\pi^-n$ as (assuming $l\leq 2$ partial waves)

$$\frac{\partial^4\sigma_{K\pi n}}{\partial s\partial\Omega\partial\Delta^2} = \frac{1}{4\pi}[|A_0|^2\rho_{00}{}^{00}+|A_1|^2(2\rho_{11}{}^{11}+\rho_{00}{}^{11})+|A_2|^2(2\rho_{22}{}^{22}+2\rho_{11}{}^{22}+\rho_{00}{}^{22})]+(1/5\pi)^{1/2}\{|A_1|^2[(\rho_{00}{}^{11}-\rho_{11}{}^{11})Y_2{}^0$$

$$+2\sqrt{3}\,\mathrm{Re}\rho_{10}{}^{11}\,\mathrm{Re}Y_2{}^1-(\sqrt{6})\rho_{1-1}{}^{11}\,\mathrm{Re}Y_2{}^2]+(\sqrt{5})\,\mathrm{Re}[A_1A_0{}^*(2\rho_{10}{}^{10}\,\mathrm{Re}Y_1{}^1+\rho_{00}{}^{10}Y_1{}^0)]$$

$$+\tfrac{1}{7}|A_2|^2[(\sqrt{5})(\rho_{22}{}^{22}-4\rho_{11}{}^{22}+3\rho_{00}{}^{22})Y_4{}^0+5(-2\rho_{22}{}^{22}+\rho_{11}{}^{22}+\rho_{00}{}^{22})Y_2{}^0-10(\mathrm{Re}\rho_{21}{}^{22}-(\sqrt{6})\,\mathrm{Re}\rho_{10}{}^{22})\,\mathrm{Re}Y_4{}^1$$

$$+2(\sqrt{3}\,\mathrm{Re}\rho_{20}{}^{22}-\sqrt{2}\,\mathrm{Re}\rho_{1-1}{}^{22})\,\mathrm{Re}Y_4{}^2-(2\sqrt{7})\,\mathrm{Re}\rho_{2-1}{}^{22}\,\mathrm{Re}Y_4{}^3+(\sqrt{14})\rho_{2-2}{}^{22}\,\mathrm{Re}Y_4{}^4-(4\,\mathrm{Re}\rho_{20}{}^{22}+(\sqrt{6})\rho_{1-1}{}^{22})\,\mathrm{Re}Y_2{}^2$$

$$-2(\mathrm{Re}\rho_{10}{}^{22}+(\sqrt{6})\,\mathrm{Re}\rho_{21}{}^{22})\,\mathrm{Re}Y_2{}^1]\}+(S\text{-}D \text{ and } P\text{-}D \text{ interference terms}),\quad(24)$$

where s, Ω, Δ^2, $\rho_{m'm}{}^{l'l}$ denote the diboson effective mass, the solid angle in the diboson rest frame, the four-momentum transfer squared to the nucleon, and the density-matrix elements for diboson states with angular momentum l' and l and helicities m' and m and where the A_l represent the lth partial-wave amplitude. Perhaps the most striking feature of the moments is the lack of variation in $Y_2{}^0$ in the $K^*(890)$ region. The explanation is that the coefficient of $Y_2{}^0$ in the above equation contains $(\rho_{00}{}^{11}-\rho_{11}{}^{11})$. The density-matrix element $\rho_{00}{}^{11}$ is primarily a measure of the pion contribution, whereas vector exchange is indicated by $\rho_{11}{}^{11}$.

When integrated over the entire Δ^2 interval the contributions roughly cancel. Note, however, that Re$Y_2{}^2$ shows sizable activity since the coefficient contains only $\rho_{1-1}{}^{11}$. The combination of π and ω exchange results in an almost isotropic K^* decay distribution in Fig. 18, but this is not true at all momentum transfers (see Fig. 13).

[32] In calculating the moments $\langle Y_l^m\rangle$, events were excluded if the four-momentum transfer squared from K^- to $\bar{K}^0\pi^-$ was greater than 1 (GeV/c)^2 or the π^-n mass was in the $\Delta(1236)$ band.

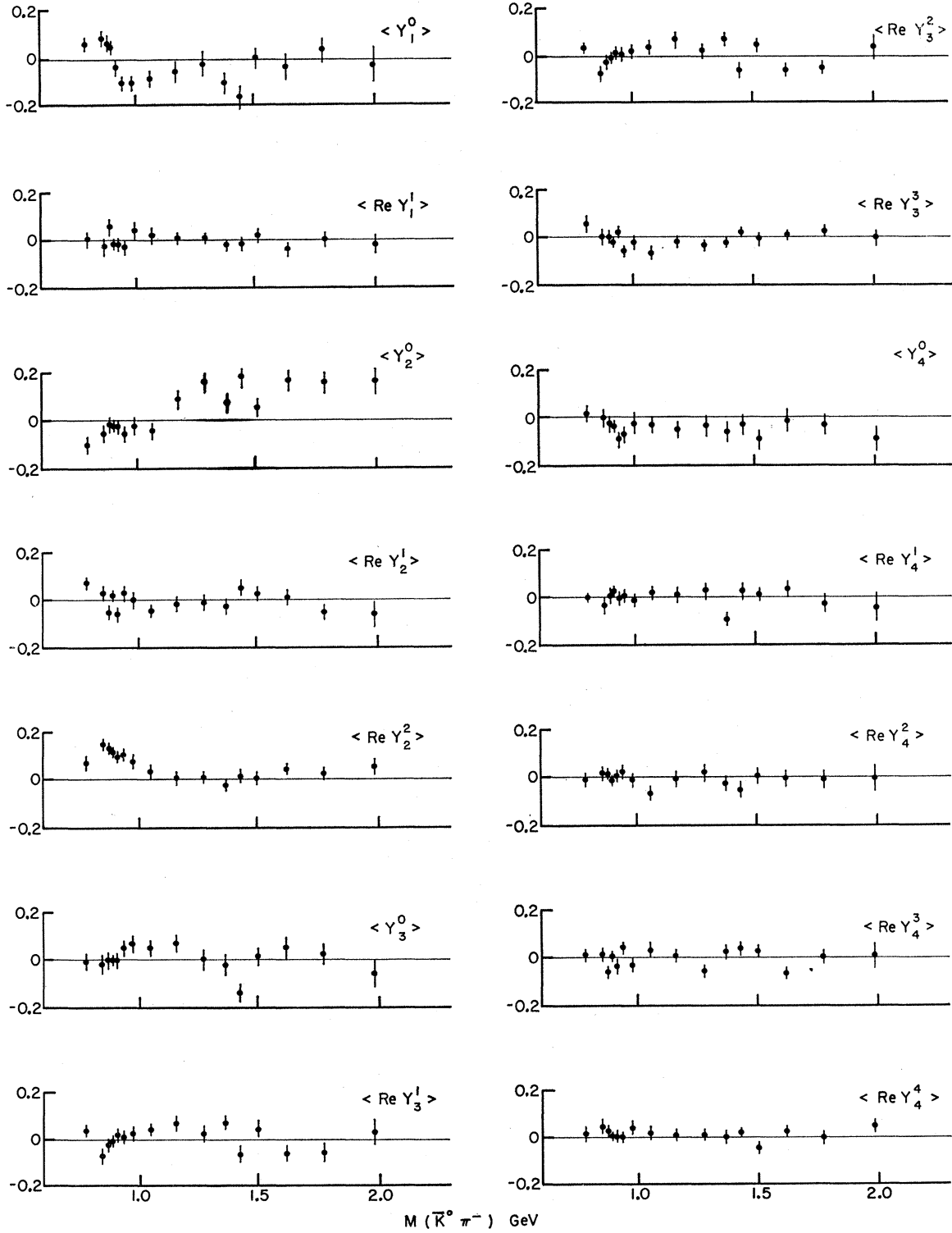[33] L. J. Gutay, F. T. Meiere, D. D. Carmony, F. T. Loeffler, and P. L. Csonka, Nucl. Phys. **B12**, 31 (1969).

FIG. 20. Spherical harmonic moments $\langle Y_l^m(\theta,\varphi) \rangle$ for $l \leq 4$ as a function of $\pi^-\bar{K}^0$ mass.

Above the $K^*(890)$, $\langle Y_2^0 \rangle$ becomes positive. This either indicates that the P wave is large and it is dominated by pion exchange or the onset of D wave or both. The only way we can have D wave (we neglect double helicity exchange) around 1420 MeV yet $\langle Y_4^0 \rangle \approx 0$ is that $\rho_{11}^{22} \cong \rho_{00}^{22}$. Pion exchange contributes to ρ_{00}^{22} and ρ_{11}^{22} arises from ω exchange. The variation of $\langle Y_1^0 \rangle$ and $\langle Y_3^0 \rangle$ indicates that there is a P-D–wave interference
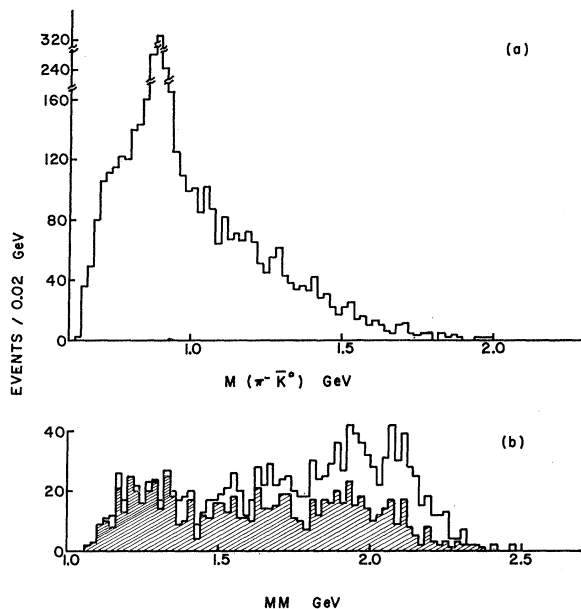
FIG. 21. Mass distributions for the reaction $K^-d \to p_s\bar{K}^0\pi^-$MM: (a) $M(\bar{K}^0\pi^-)$; (b) missing mass produced with the $K^*(890)$; the shaded area corresponds to events with $-t < 1.0$ $(\text{GeV}/c)^2$.

suggesting the possibility of a P-wave enhancement around 1200–1300 MeV produced by pion exchange as well as the known D-wave enhancement around 1420 MeV.

IV. FINAL STATE $K^-d \to p_s\bar{K}^0\pi^-$ MM

The missing mass in the reaction

$$K^-d \to p\bar{K}^0\pi^-\text{MM} \qquad (4)$$

is shown in Fig. 3. There is evidence for $\Delta^0(1236)$
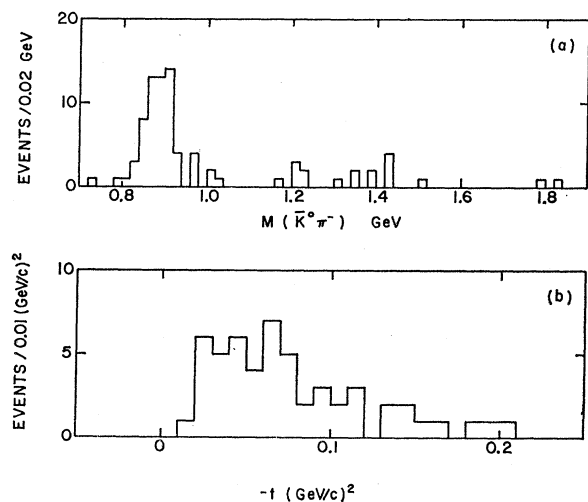

FIG. 22. (a) The $\bar{K}^0\pi^-$ effective mass in the reaction $K^-d \to d\bar{K}^0\pi^-$. (b) The four-momentum transfer distribution between the incident K^- and the $K^*(890)$.

TABLE V. Cross sections for various channels.

Reaction	Number of events	Cross section (μb)
$K^-d \to d\pi^-\bar{K}^0$	83	48±8
$\to K^*(890)d$	50±12	29±7
$\to K^*(1420)d$	5±2	3±1
$K^-d \to d\pi^-\bar{K}^0\pi^0$	246	140±38
$\to d^{*0}K^{*0}$	12±6	7±3
$\to d^{*+}K^{*-}$	23±9	13±5
$K^-d \to p_s\pi^-\bar{K}^0$MM	4074	2340±36
$p_sK^*(890)$MM	560±140	320±80
$p_s\pi^-\bar{K}^0\Delta^0(1236)$	174±50	100±30
$p_sK^*(890)\Delta^0(1236)$	110±30	63±17

production. The $\bar{K}^0\pi^-$ effective-mass spectrum is shown in Fig. 21(a) and a strong $K^*(890)$ signal is apparent. We have attempted to isolate K^-n quasi-two-body production by requiring that the proton have a momentum less than 0.3 GeV/c and by requiring a $K^*(890)$.[16] The resultant missing mass is shown in Fig. 21(b). The shaded histogram shows the missing mass when the momentum transfer to the $K^*(890)$ is less than 1.0 (GeV/c).[2] Peripheral production of $K^{*-}(890)\Delta^0(1236)$ is observed with a cross section of 63±17 mb (see Table V).

V. FINAL STATE $K^-d \to \bar{K}^0\pi^-d$

We have studied the reaction

$$K^-d \to \bar{K}^0\pi^-d \qquad (2)$$

in which the deuteron remains intact after the interaction. We identified 83 events which fit this seven-constraint fit. A detailed analysis based on part of this sample has already been reported[4] (see also Table V). The $\bar{K}^0\pi^-$ effective-mass spectrum is given in Fig. 22(a). Strong $K^{*-}(890)$ resonance production contributes to approximately 60% of the final state (2). There may also be a small signal from the $K^*(1420)$.

If we assume that $K^*(890)$ production can be represented by a simple one-particle-exchange diagram, then
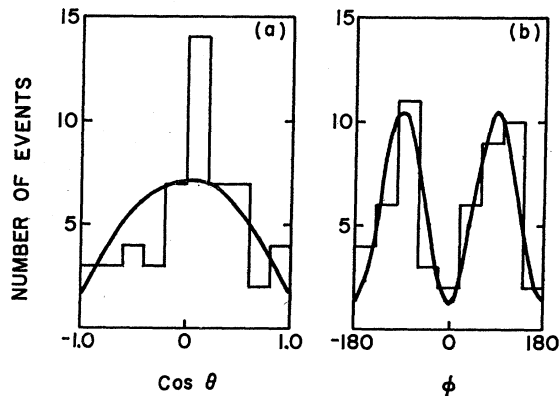

FIG. 23. Cosθ and φ distributions of the $K^*(890)$ decay in the reaction $K^-d \to d\bar{K}^0\pi^-$. The solid curves are calculated from the density-matrix elements.

the zero isotopic spin of the deuteron limits the exchanged particle to be an isoscalar object. The ω meson is the most likely candidate.[4] This channel, then, isolates the vector exchange contribution to $K^*(890)$ production. Figure 22(b) gives the momentum-transfer distribution from the incident K^- to the outgoing $\bar{K}^0\pi^-$ system. The depletion of events in the first bin comes from low-momentum (<150 MeV/c) deuterons which are not visible in the bubble chamber. We have not made a scanning-bias correction because of the small number of events in each momentum bin. Nor did we extrapolate to the unseen region because of the possibility of the physical effects (e.g., production mechanisms) being different from the visible region. Very
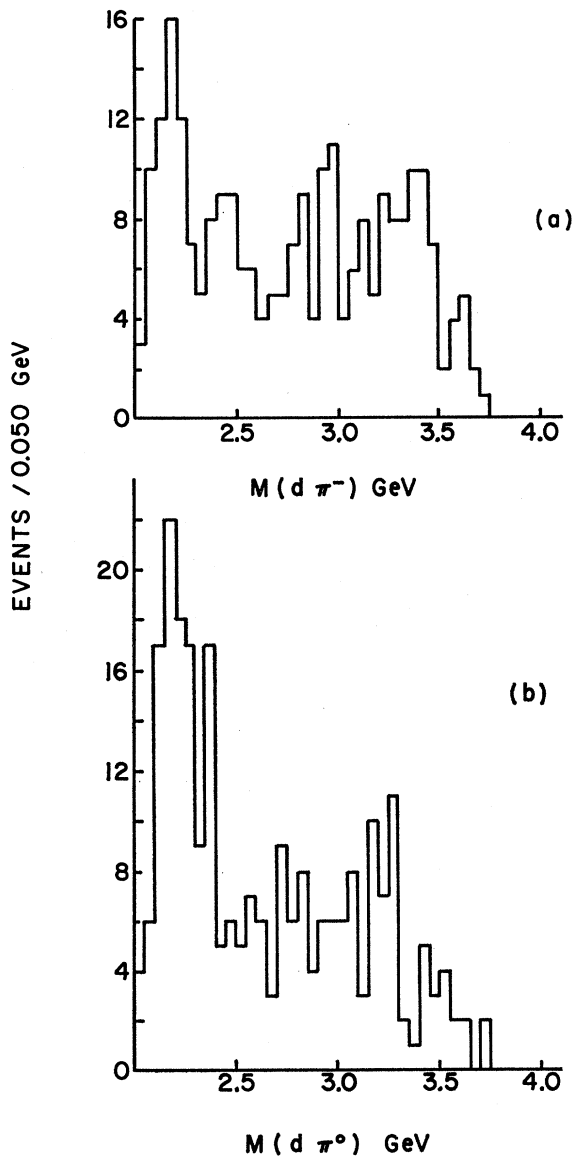

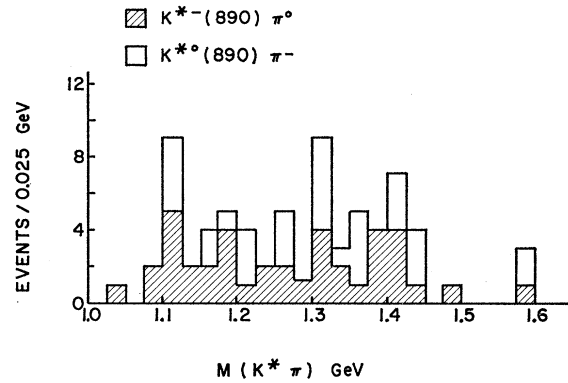FIG. 25. $K^*(890)\pi$ effective-mass distribution for events whose $d\pi$ effective mass falls outside the d^* band in the reaction $K^-d \to \bar{K}^0\pi^-\pi^0 d$.

large momentum transfers are inhibited by the breaking up of the weakly bound deuteron as well as by the scanning criteria which limited the positive track from the primary vertex to be less than 15 cm long.

ω exchange combined with the assumption of neglecting off-mass-shell and absorption effects leads one to

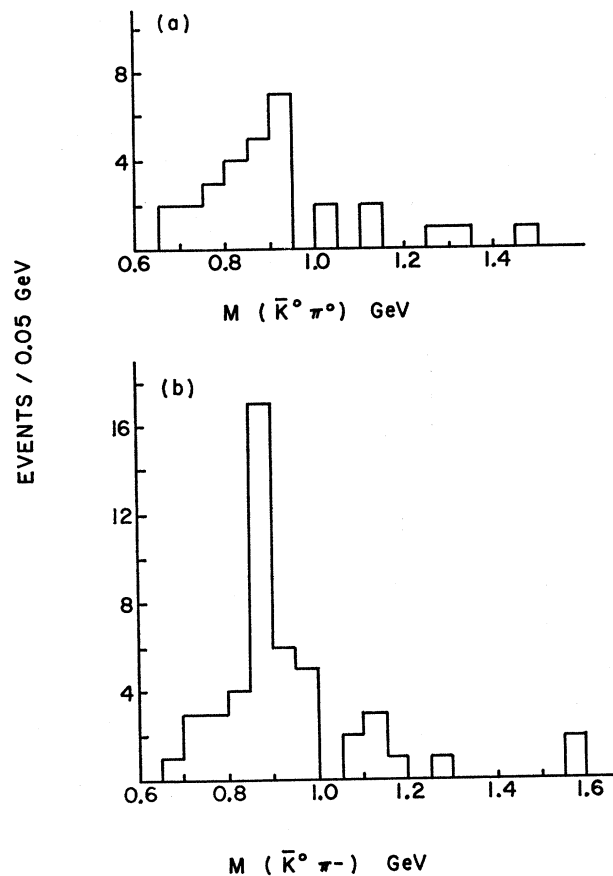FIG. 24. Effective-mass distributions for the reaction $K^-d \to \bar{K}^0\pi^-\pi^0 d$: (a) $d\pi^-$; (b) $d\pi^0$.

FIG. 26. $\bar{K}\pi$ effective-mass spectrum from the reaction $K^-d \to d^*\bar{K}^0\pi$: (a) $M(\bar{K}^0\pi^0)$; (b) $M(\bar{K}^0\pi^-)$.

expect that the ρ_{00} density-matrix element would be zero, giving a $\sin^2\theta$ decay angular distribution (θ is defined as the angle between the incident K^- to the outgoing $\bar{K}^0$ in the $\bar{K}^0\pi^-$ rest frame) and that the density-matrix element $\mathrm{Re}\rho_{10}$ would also be zero.

The density-matrix elements as determined by the method of moments are $\rho_{00}=0.09\pm0.09$, $\mathrm{Re}\rho_{10}=0.01$ ±0.04, and $\rho_{1-1}=0.39\pm0.08$ in good agreement with vector exchange. Figure 23 gives the $\cos\theta$ and φ (φ is the azimuthal angle in the $\bar{K}^0\pi^-$ rest frame) projections of the $K^*(890)$ decay angular distribution. The curves are calculated from the above density-matrix elements.
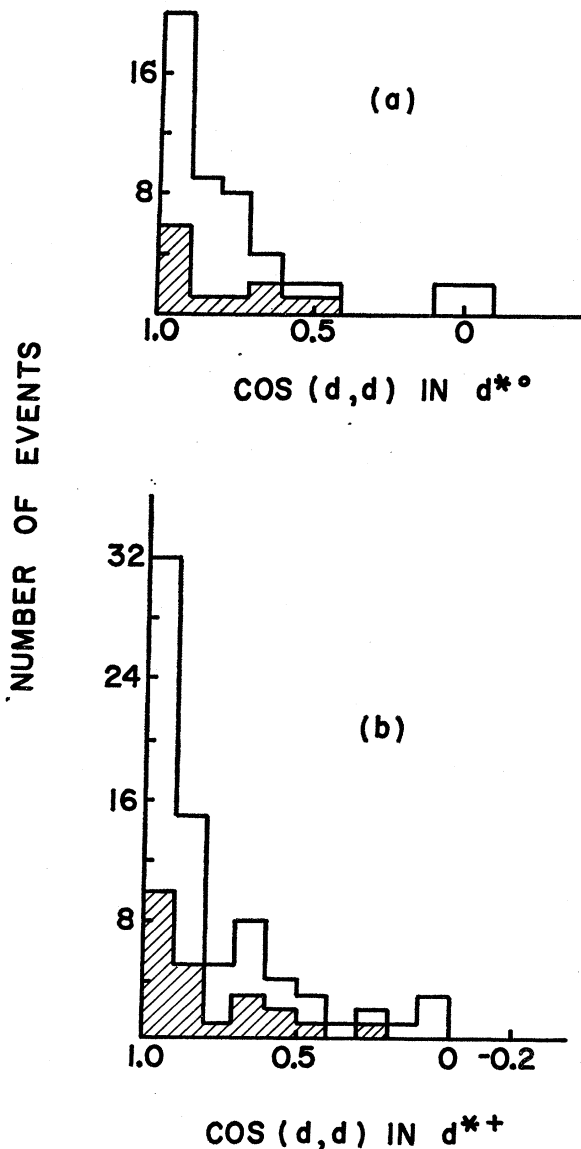
VI. FINAL STATE $K^-d \rightarrow \bar{K}^0\pi^-\pi^0d$

The final state

$$K^-d \rightarrow \bar{K}^0\pi^{-0}d \qquad (3)$$

is complicated by possible production of $K^{*-}(890)$, $K^{*0}(890)$, d^{*0}, and d^{*+}, and three-body final-state enhancements in the $K\pi\pi$ system as well as considerable uncertainty as the amount or effect of the background from other reactions.

The d^* effect was first seen in a π^-d production experiment.[34] It shows up as a peak in the πd effective-mass spectrum at a mass of about 2.17 GeV with a width of approximately 0.1 GeV. The highly asymmetric decay of the d^* in its rest frame implied that the effect could not be interpreted as a resonance. It was suggested that the d^* was $\Delta(1236)$-N state which decays in such a manner that the two outgoing nucleons remain a deuteron. Thus the effect is associated with a peak in the cross section for $\pi^+d \rightarrow pp$ at a center-of-mass energy equal to the d^* mass.[35] In Fig. 24 we show the $d\pi^-$ and $d\pi^0$ effective-mass spectrum for all events in the sample. The d^* enhancement is in evidence in both distributions.

Recent experiments have noted structure in the $K\pi\pi$ effective-mass region between 1.1 and 1.5 GeV. Resonances have been reported at 1.25, 1.36, and 1.42 GeV [36] with large branching ratios into $K^*\pi$. In Fig. 25 we show the $K^*\pi$ effective-mass distribution for events whose $d\pi$ effective mass falls outside the d^* band.[37] We find no significant enhancements. This reaction has also been reported on at 12.6 GeV/c.[38]

Figure 26 shows the $\bar{K}^0\pi^0$ and $\bar{K}^0\pi^-$ effective-mass spectrum from the reactions

$$K^-d \rightarrow \bar{K}^0\pi^-d^{*+} \qquad (25)$$

and

$$K^-d \rightarrow \bar{K}^0\pi^0d^{*0}. \qquad (26)$$

Figure 27 gives the angle between the target deuteron and the outgoing deuteron in the d^* rest frame for all d^* events. The shaded areas corresponds to K^*d^* production. The asymmetric decay of the d^* system has been taken as evidence for some type of simple one-pion-exchange mechanism. The decay distribution resembles that of the πd elastic scattering cross section at a total center-of-mass energy of 2.2 GeV.[39] The asymmetry of both d^*'s is evident in Fig. 27. The observed number of $d^{*0}K^{*0}$ events should be equal to

FIG. 27. Cosine of the angle between the incident and outgoing deuteron in the d^* rest frame in the reaction $K^-d \rightarrow d^*\bar{K}^0\pi$. The shaded area corresponds to K^*d^* events. (a) d^{*0} events; (b) d^{*+} events.

[34] M. A. Abolins, D. D. Carmony, R. L. Lander, and Ng.-h. Xuong, Phys. Rev. Letters **15**, 125 (1965).

[35] B. S. Neganov and L. B. Parfenov, Zh. Esperim. i Teor. Fiz. **34**, 767 (1958) [Soviet Phys.—JETP **7**, 528 (1958)].

[36] G. Goldhaber, A. Firestone, and B. C. Shen, Phys. Rev. Letters **19**, 972 (1967).

[37] The d^* enhancement region is defined to be $2.1 \le M(d\pi) \le 2.3$ GeV.

[38] D. Denegri, A. Callahan, L. Ettlinger, D. Gillepsie, G. Goodman, G. Luste, R. Mercer, E. Moses, A. Pevsner, and R. Zdanis, Phys. Rev. Letters **20**, 1194 (1968).

[39] E. G. Pewitt, T. H. Fields, G. B. Yooh, J. G. Fetkovich, and M. Derrick, Phys. Rev. **131**, 1826 (1963).

the number of $d^{*+}K^{*-}$ events if one-pion exchange is the dominant production process. We find that $\sigma(K^-d \to K^{*0}d^{*0})/\sigma(K^-d \to K^{*-}d^{*+}) = 0.5 \pm 0.4$, which is not inconsistent with 1, especially since the effects of contamination from other final states on this channel are not understood. A better place to investigate the d^*-K^* state would be in the reaction

$$K^-d \to K^-\pi^+\pi^-d, \qquad (27)$$

which is a four-constraint fit, and in which only one $K^*(890)$ is allowed.

ACKNOWLEDGMENTS

Measurement of the Velocity Dependence of the Helicity of Beta Particles from Co60†

D. M. LAZARUS* AND J. S. GREENBERG

Physics Department, Yale University, New Haven, Connecticut 06520

(Received 13 March 1970)

A series of experiments has been carried out to study the velocity dependence of the helicity $\mathcal{K}$ of β particles from the allowed Gamow-Teller decay in Co60. The energies examined were varied from 205 keV ($v/c=0.7$) to 50 keV ($v/c=0.41$), a region where the velocity is changing rapidly with energy, and where several other measurements have reported deviations from $\mathcal{K} = -v/c$. We have not observed any discrepancy with a $-v/c$ dependence for the helicity within a measurement accuracy of a few percent at the highest velocities and 9% at the lowest velocity. The weighted mean of the helicity measurements is $-\mathcal{K}/(v/c) = 1.014 \pm 0.018$. Assuming, in turn, either the two-component neutrino theory with predominantly axial-vector interaction or the absence of any tensor interaction admixture, this result limits the ratio C_T/C_A to <0.0029, and the ratio C_A'/C_A to values between 0.90 and 1.11. The helicity was analyzed by Mott scattering after transformation of the polarization from longitudinal to transverse. A screened Mott scattering function $S(\theta)$ was used in the analysis. The behavior of depolarization effects and the other systematic errors associated with the technique as a function of β-particle energy was investigated extensively, and the influence of these effects on the results is reported.

I. INTRODUCTION

THE $V-\lambda A$ form for the four-fermion interaction provides a consistent representation for the extensive experimental information now available on the strangeness-conserving weak decays.[1-7] At low energy, investigations in nuclear β decay of spectral shapes, ft values, β-ν correlations, the β asymmetry from polarized nuclei, β-γ (circular polarization) correlations' the helicity of the neutrino, and the helicity of β par-

---

[1] T. D. Lee and C. S. Wu, Ann. Rev. Nucl. Sci. **15**, 381 (1965).

[2] C. S. Wu, Rev. Mod. Phys. **31**, 783 (1959); **36**, 618 (1964).

[3] M. Deutsch and O. Kofoed-Hansen, in *Experimental Nuclear Physics*, edited by E. Segrè (Wiley, New York, 1959), Vol. 3.

[4] E. J. Konopinski, Ann. Rev. Nucl. Sci. **9**, 99 (1959).

[5] R. J. Blin-Stoyle, in Proceedings of the Topical Conference on Weak Interactions, CERN, 1969, p. 497 (unpublished).

[6] *Alpha-, Beta-, and Gamma-Ray Spectroscopy*, edited by Kai Seigbahn (North-Holland, Amsterdam, 1965), Vol. 2, Chaps. XXIII-XXIV.

[7] References 1–6 are review articles. References to original work are given there.

ticles have furnished some of the definitive tests for the $V-\lambda A$ theory with conserved vector current and maximum parity violation, and have determined a number of its important parameters. We may note, however, that there is considerable experimental uncertainty associated with the measurements of some of these parameters which allows for significant departures from the predictions of the theory. These uncertainties reflect, in part, the difficulties of the measurements, and in some cases the poor sensitivity with which the β-decay parameters can be extracted from the measured quantities noted above.

The latter situation, for example, occurs in the determination of the relative magnitudes of the parity-conserving and the parity-nonconserving coupling constants, C'/C. It is a characteristic feature of the experiments from which this ratio may be deduced that the functional dependence of the measured pseudoscalar quantities on the ratio C'/C always occurs in the form

$$\frac{C'/C}{1+(C'/C)^2},$$